Development (2015) 142, 910-920 doi:10.1242/dev.116996

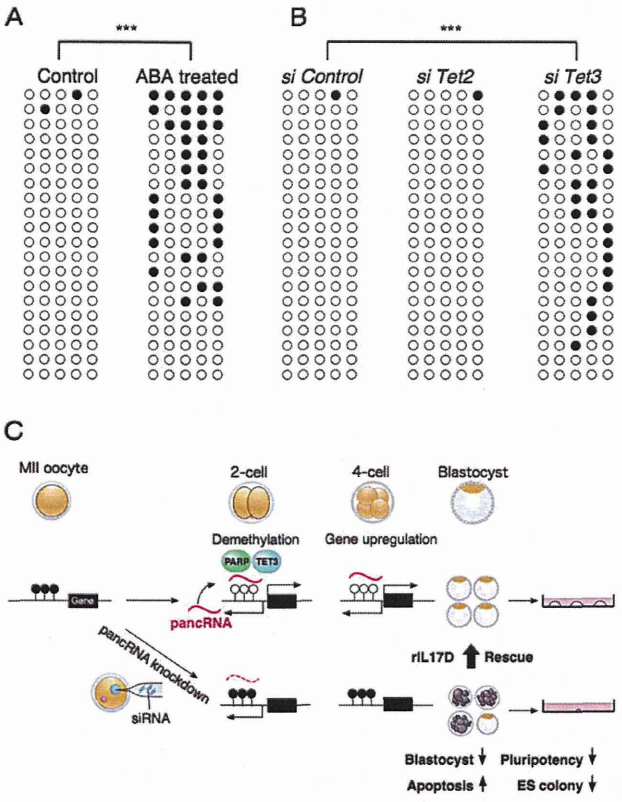


**Fig. 6. Epigenetic changes accompanying zygotic pancRNA-mediated gene activation during early mouse development.** (A) DNA methylation status of ABA-treated 2-cell embryos. (B) DNA methylation status of *Tet2* or *Tet3* versus control siRNA-injected embryos. ***$P$<0.001. (C) A model for pancRNA-mediated gene activation in early mouse development. At the 2-cell stage, *pancIl17d* expression, together with TET3 and PARP, leads to establishment of the hypomethylated status at the *Il17d* promoter in a sequence-specific manner, and thus to *Il17d* mRNA expression starting from the 4-cell stage. When these steps are compromised, apoptosis increases and cell proliferation decreases, adversely affecting embryonic development.

## Sequence-specific transcriptional activation mediated by pancRNAs

There have been several reports on the molecular basis of lncRNA-mediated transcriptional regulation in *trans* [for a review see Fatica and Bozzoni (2014)]. For example, *HOTAIR* represents a set of lncRNAs that can influence dispersed genomic regions (Chu et al., 2011). By contrast, we now think that a single pancRNA acts to mediate corresponding gene activation in *cis*: knockdown of *pancIl17d*, *pancMospd3* or *pancTbc1d22a* resulted in downregulation of the partner gene, and this downregulation was accompanied by a hypermethylated status of the corresponding promoter regions (Fig. 3A,B). In addition, we found that *pancIl17d* expression preceded *Il17d* expression (Fig. 2B; supplementary material Fig. S15), also supporting the notion that the pancRNA epigenetically activates its partner gene in *cis*. However, we cannot completely exclude the possibility that a pancRNA affects expression of other genes in *trans*. Nonetheless, we believe that the *trans* effect, if any, on preimplantation development was relatively small, because several developmental defects caused by knocking down *pancIl17d* were rescued by addition of rIL17D protein. These findings strongly support the idea that a pancRNA specifically regulates expression of the gene with which it shares a bidirectional promoter region.

## The mechanism of pancRNA-triggered gene activation

One possible scenario is that gene activation-associated pancRNAs specify the genomic position for establishing an epigenetic status that is conducive to gene activation with TET3 and BER components (Fig. 6A,B), which are involved in genome-wide DNA demethylation (Branco et al., 2012; Hajkova et al., 2010). However, we do not yet know what factors initiate the expression of gene activation-associated pancRNAs. In this study, we tried to identify such factors and found strand-specific enrichment of a CT-rich motif in a set of zygotic pancRNA-partnered genes (Fig. 1F). The TSSs of the pancRNA-partnered genes provide the switching points for the observed asymmetric distribution of the CT-rich motif (supplementary material Fig. S5). Considering the divergent transcription of mRNA and pancRNA, the distribution pattern of this CT-rich motif seems to be preferentially located upstream of both pancRNAs and mRNAs. This raises the possibility that the coordinated expression of pancRNAs and mRNAs is regulated by similar machineries. This hypothesis is supported by the fact that the expression of 426 out of 568 pancRNAs increased at the 2-cell stage concomitantly with the increase in corresponding mRNA expression (supplementary material Fig. S3). However, the factor that binds to this CT-rich motif remains to be identified; indeed, the CT-rich motif is present upstream of *pancIl17d* and *pancTbc1d22a*, but not *pancMospd3*, and therefore information on additional sequence motifs and their binding factors will be needed to clarify the driving force that reprograms the chromatin structure in conjunction with pancRNA activation.

Although the pancRNA expression change seems to coincide with the DNA methylation change during preimplantation development, the effect on DNA methylation might be exerted indirectly. For example, DNA methylation and histone modification work together in gene silencing, and pancRNAs might initially affect some epigenetic/transcriptional environmental condition, such as histone modification status, leading to the DNA demethylation. Further advances in histone modification analysis techniques will enable us to dissect the exact kinetics of epigenetic changes triggered by pancRNA expression and thus aide in the identification of the molecular complex(es) that functions with pancRNA for sequence-specific gene activation.

## Developmental roles of pancRNAs

It is clear that the *pancIl17d-Il17d* pair performs some functions at the preimplantation stage. We speculate that some of the other upregulated pancRNA/gene pairs affect embryonic development. Several lncRNAs have also been shown to be involved in mouse postimplantation development [for a review see Fatica and Bozzoni (2014)]. For example, knockout mice of the lncRNA *Fendrr*, which is derived from the promoter region of *Foxf1*, die around embryonic day 14 due to impairment of heart development. Although knockdown of *pancMospd3* did not cause any detectable developmental defects in blastocyst formation (Fig. 3C), it must function thereafter, since mice lacking the *Mospd3* gene display neonatal lethality with defects of heart development (Pall et al., 2004). This notion is supported by our data showing that *pancMospd3* knockdown caused failure of hatching from the zona pellucida (supplementary material Fig. S10).

Interestingly, cell death-related genes were enriched among co-upregulated pancRNA-partnered genes (supplementary material Tables S1 and S2). These include *Bag6*, *Pdcd2*, *Map3k7* and *Fadd*,

Development (2015) 142, 910-920 doi:10.1242/dev.116996

which are essential for embryonic development (Fabian et al., 2005; Jadrich et al., 2006; Mu et al., 2010; Yeh et al., 1998). For example, *Bag6* knockout mice die with defects of kidney, lung and brain formation as a result of dysregulation of apoptosis and cell proliferation (Fabian et al., 2005). In accord with this, our *pancBag6* knockdown experiment showed increased cell death among ESCs (supplementary material Fig. S16). Therefore, pancRNAs seem to be produced at a significant number of gene promoters that should be regulated according to the developmental context.

This raises the intriguing question of why pancRNAs are employed within the developmental gene regulation network. One possibility is that pancRNAs have been adopted to increase the complexity of the regulatory network system. The novel layer of transcriptional regulation imposed by the acquisition of pancRNAs might have contributed to generating numerous varieties of gene expression patterns during development (Imamura et al., 2014). Recently, it has been reported that lncRNAs, including pancRNAs, are frequently regulated by developmentally important factors, such as homeobox proteins, (Necsulea et al., 2014), supporting our idea that pancRNAs acts together with other regulatory factors for complex and orchestrated developmental gene regulation.

The knockdown of *pancTbc1d22a* and *pancBag6* did not cause marked defects in preimplantation development. As described above, pancRNAs function in the regulation of many biological processes according to their partner genes. In fact, *Tbc1d22a* belongs to the TBCK gene family, whose members are thought to act as GTPase-activating proteins and to influence cell proliferation through mTOR signaling (Alexander et al., 2013; Liu et al., 2013). Thus, although *Tbc1d22a* might have a role during development, it is possible that paralogs of *Tbc1d22a* might compensate for the knockdown effect. The same might be true for *pancBag6*, the knockdown of which resulted in only a slight decrease in ESC number (supplementary material Fig. S16).

### Conclusion

We conclude that gene activation-associated pancRNA provides a new layer of epigenetic regulation during mammalian development.

## MATERIALS AND METHODS

### Preparation of oocytes, embryos, sperm and ESCs

MII oocytes were obtained from the oviducts of 7- to 8-week-old F1 mice (C57BL/6×C3H) induced to superovulate by intraperitoneal injection of 5 IU of pregnant mare serum gonadotropin (Asuka), followed 48 h later by injection of 5 IU of human chorionic gonadotropin (hCG, Asuka). Embryos were obtained after mating the superovulated females with F1 males. Oocytes and zygotes were recovered in M2 medium (Sigma) 17 h after hCG injection, and then, following removal of cumulus cells with 0.03% hyaluronidase (Sigma), they were either subjected to direct methylation analysis and RNA analysis, or cultured in M16 medium (Sigma) at 37°C under 5% $CO_2$/air for the collection of fertilized embryos. Sperm were obtained from F1 male epididymis, and motile sperm of good quality were selected by the direct swim-up method (Younglai et al., 2001). The embryos were treated with ABA (Sigma) as previously described (Imamura et al., 2004a). Blastocysts were plated in N2 medium containing B27 (Invitrogen), 2-mercaptoethanol (Wako), GlutaMAX-I (Gibco), bovine serum albumin fraction V (Sigma), LIF (Millipore), PD0325901 (Sigma) and CHIR99021 (Axon) (2i medium) (Ying et al., 2008) and cultured for 10 days. ESC-like colonies were processed for immunohistochemistry. ESCs were cultured on a 0.1% gelatin-coated dish in a 37°C incubator under 5% $CO_2$/air, and propagated by trypsinizing and replating every 2 or 3 days. EB formation and *in vitro* hatching are described in the supplementary methods.

### Directional RNA-seq library preparation

Total RNA and poly(A)$^+$ RNA were extracted from pools, each of which contained 100 MII oocytes, 2-cell embryos (C57/B6×ICR), control siRNA-injected morula embryos or *pancIl17d* knockdown morula embryos, using the Dynabeads mRNA DIRECT Micro Kit (Invitrogen). Four replicates were made for directional RNA-seq library construction using the NEBNext Ultra Directional RNA Library Prep Kit for Illumina (NEB). In this library preparation, cDNAs were enriched by 15-cycle PCR. Illumina HiSeq 2000 was used to perform 50 bp single-end sequencing according to the manufacturer's instructions. RNA-seq data have been deposited in the DDBJ Sequence Read Archive (DRA) under accession number DRA002400.

### Data mining

Sequencing reads obtained from our directional RNA-seq (DRA: DRA002400) and publicly available data [NCBI Sequence Read Archive (SRA)] for ESCs (SRA:SRR315596) were assessed with the FASTX tool kit (Patel and Jain, 2012) to remove short (<20 bp) and low quality (quality score <20) reads, followed by trimming of the adaptor sequence.

Preprocessed reads were mapped to the mouse mm10 genome using TopHat2/Bowtie2 (Kim et al., 2013). Cufflinks and Cuffdiff (Trapnell et al., 2012) were used for the reads per kb of exon model per million mapped reads (RPKM) calculation and differential expression analyses. For pancRNA quantification, we counted only reads that mapped to the antisense sequences of the promoter regions (−1000 to −1 bp from the TSS) of genes, because pancRNAs corresponding to antisense sequences of the promoter regions show the potential to increase mRNA production (Tomikawa et al., 2011; Uesaka et al., 2014). If a promoter region overlapped with another RefSeq gene, the promoter was excluded from the dataset to avoid contamination of the pancRNA pool by protein-coding genes. Hierarchical clustering of sequenced samples based on gene expression levels was drawn using the cummeRbund package (http://rgm3.lab.nig.ac.jp/RGM/R_package_list). For motif searches within the promoter sequences, ≥10-fold upregulated pancRNAs in 2-cell embryos were selected by comparing their levels with those in MII oocytes. The −200 to −1 bp sequences (relative to the TSS) of 370 corresponding mRNAs were examined using rGADEM, one of the Bioconductor packages (Gentleman et al., 2004). To verify the presence of a motif in the pancRNA-partnered gene loci, we further extracted and counted genes that possessed or lacked sequences showing 90% or more identity to the candidate motif using the matchPWM program in the Biostrings package (Pages et al., 2013). pancRNA-mRNA sets subjected to the experiments described below were selected based on the following criteria: RPKM <0.5 in MII oocytes, RPKM >1 in 2-cell embryos and ESCs (supplementary material Table S3).

### PCR detection of pancRNA and mRNA

To quantify the pancRNA and mRNA expression levels in the embryos, we purified total RNAs from sperm, oocytes, and fertilized 1-cell (corresponding to 30 h after hCG injection), 2-cell (44 h) and 4-cell (54 h) embryos using the Dynabeads mRNA DIRECT Micro Kit and subjected them to reverse transcription. For ESCs, 3 µg total RNA that had been extracted using TRIzol (Invitrogen) was utilized for reverse transcription with SuperScript III (Invitrogen) reverse transcriptase. The synthesized cDNAs were subjected to qPCR using the KAPA SYBR Fast qPCR Kit (KAPA Biosystems). The primers used in these analyses are listed in supplementary material Table S6. *Gapdh* was used as an internal control.

### Bisulfite sequencing

To determine the DNA methylation profiles of the *Il17d*, *Mospd3* and *Tbc1d22a* promoter regions, sample pools consisting of genomic DNA from 20-50 oocytes or embryos were subjected to the bisulfite reaction using the MethylCode Kit (Invitrogen) according to the manufacturer's instructions. Each bisulfite-treated genome was amplified using AmpliTaq Gold 360 Master Mix (Life Technologies) or EpiTaq HS (TaKaRa) and the specific primers listed in supplementary material Table S6. In order to avoid PCR bias, we subcloned more than five PCR bands as previously described (Imamura et al., 2005), and performed bisulfite sequencing of more than 20 of the resulting subclones, for each sample. Visualization of MethylC-seq data is described in the supplementary methods.

Development (2015) 142, 910-920 doi:10.1242/dev.116996

### pancRNA knockdown and overexpression experiments

We microinjected 5-10 pl of 2 μM siRNA that targeted pancRNA of *Il17d*, *Mospd3* or *Tbc1d22a* (supplementary material Table S7), together with 5 ng/μl N2-EGFP vector (Clontech), into the pronuclei of fertilized embryos 21 h after hCG injection. In a rescue experiment of siRNA knockdown, 5 ng/μl *pancIl17d* overexpression construct [−706 bp to −418 bp relative to the TSS of *Il17d* in pRC/CMV (Invitrogen)] was simultaneously microinjected into the pronuclei. In the case of siRNAs that targeted *Tet2* and *Tet3* mRNAs, 5-10 pl of each siRNA at 50 μM was injected into the cytoplasm of embryos 14 h after hCG injection. As a negative control for siRNA experiments, we used the MISSION siRNA universal negative control (Sigma). siRNA-injected embryos were used for DNA methylation and RNA analyses. To look for possible morphological changes, *in vitro* culture was continued for 3 more days. In some cases, recombinant IL17D (R&D Systems) was added to a final concentration of 100 ng/ml at the 4-cell stage.

For knockdown experiments, ESCs were transfected with each siRNA (100 nM final concentration) as listed in supplementary material Table S7, together with pEGFP-N2 vector (Clontech), by electroporation with the Neon Transfection System (Invitrogen). At 24 h after transfection, cells were used for TUNEL assay, EdU labeling assay or RT-qPCR. For longer duration knockdown experiments in ESCs, pLLX-shRNA expression vectors, which were generously provided by Drs Z. Zhou and M. E. Greenberg (Lois et al., 2002; Zhou et al., 2006) and were modified to express GFP together with a puromycin resistance gene under the ubiquitin C promoter, were prepared as listed in supplementary material Table S7. Human embryonic kidney cells were used as producers of lentiviruses that contained the modified pLLX-shRNA expression vectors. After 2 days of infection, ESCs were selected with puromycin for 3 days to check their phenotypes.

### Cell staining

Immunohistochemistry was performed as follows: fixation with 4% PFA for 20 min at room temperature; washing twice in PBS; permeabilization and blocking in blocking buffer (0.1% Triton X-100 and 3% FBS in PBS) for 1 h at room temperature; overnight incubation with primary antibodies diluted 1/500 in blocking solution; washing three times in PBS; incubation with Hoechst 33258 (Nacalai Tesque) and secondary antibody diluted 1/500 in blocking solution for 1 h in the dark at room temperature; and washing three times in PBS. Imaging was performed with a Leica AF6000 microscope. The primary antibody mouse anti-CDX2 (MU392A-UC, BioGenex) was used for immunostaining. CF488A donkey anti-mouse IgG (Biotium) secondary antibody was used to visualize signals. For the TUNEL assay, cells were stained with TMR Red using the *In Situ* Cell Death Detection Kit (Roche) according to the manufacturer's instructions. For the EdU assay, EdU of the Click-iT EdU Imaging Kit (Invitrogen) was added to the ESC culture medium by exchanging half the medium and culturing for 4 h; the cells were then fixed with 4% PFA, permeabilized with 0.1% Triton X-100 in PBS, and stained with 1× Click-iT Reaction Buffer and Hoechst 33258.

### Statistical analysis

All data are reported as the mean±s.e.m. Student's *t*-test was used for comparisons between two groups. Unless there is a specific statement about the number of replicates, three replicates were analyzed for each experiment. Tukey's multiple comparison test was used for comparisons among three or more groups. The Mann–Whitney *U*-test was used to compare DNA methylation levels among samples.

#### Acknowledgements

We thank Osamu Nishimura and Yutaka Suzuki for transcriptome analysis; Eri Kawaguchi for DNA sequencing; Yuichi Shima, Teppei Goto and Masumi Hirabayashi for embryo manipulation; Tsukasa Sanosaka and Sayako Katada for experimental advice; Naoki Yamamoto, Kota Onoda and Hirofumi Noguchi for many discussions; and Elizabeth Nakajima and Ian Smith for proofreading the manuscript.

#### Competing interests

The authors declare no competing or financial interests.

#### Author contributions

N.H. conceived the project, designed and performed experiments, conducted bioinformatic analysis and drafted the manuscript. M.U. conducted bioinformatic analysis. K.N. and K.A. designed experiments and drafted the manuscript. T.I. conceived the project, designed experiments, conducted bioinformatic analysis, coordinated the study and drafted the manuscript. All authors read and approved the final manuscript.

#### Funding

This work was in part supported by Grants-in-Aid [Nos. 25660250 and 25132706] to T.I. from Japan Society for the Promotion of Science (JSPS), Global COE program A06 (to Kyoto University) and a Grant-in-Aid [No. 221S0002] for Scientific Research on Innovative Areas 'Genome Science' from the Ministry of Education, Culture, Sports, Science and Technology (MEXT), and the Asahi Glass Foundation to T.I. N.H. is supported by a JSPS Research Fellowship. Deposited in PMC for immediate release.

#### Supplementary material

Supplementary material available online at
http://dev.biologists.org/lookup/suppl/doi:10.1242/dev.116996/-/DC1

#### References

**Alexander, S. P. H., Benson, H. E., Faccenda, E., Pawson, A. J., Sharman, J. L., Spedding, M., Peters, J. A. and Harmar, A. J.; CGTP Collaborators** (2013). The concise guide to PHARMACOLOGY 2013/14: enzymes. *Br. J. Pharmacol.* **170**, 1797-1867.

**Aoki, F., Worrad, D. M. and Schultz, R. M.** (1997). Regulation of transcriptional activity during the first and second cell cycles in the preimplantation mouse embryo. *Dev. Biol.* **181**, 296-307.

**Borgel, J., Guibert, S., Li, Y., Chiba, H., Schübeler, D., Sasaki, H., Forné, T. and Weber, M.** (2010). Targets and dynamics of promoter DNA methylation during early mouse development. *Nat. Genet.* **42**, 1093-1100.

**Branco, M. R., Ficz, G. and Reik, W.** (2012). Uncovering the role of 5-hydroxymethylcytosine in the epigenome. *Nat. Rev. Genet.* **13**, 7-13.

**Braun, R. E.** (2001). Packaging paternal chromosomes with protamine. *Nat. Genet.* **28**, 10-12.

**Brison, D. R. and Schultz, R. M.** (1997). Apoptosis during mouse blastocyst formation: evidence for a role for survival factors including transforming growth factor alpha. *Biol. Reprod.* **56**, 1088-1096.

**Chambers, I., Colby, D., Robertson, M., Nichols, J., Lee, S., Tweedie, S. and Smith, A.** (2003). Functional expression cloning of Nanog, a pluripotency sustaining factor in embryonic stem cells. *Cell* **113**, 643-655.

**Chu, C., Qu, K., Zhong, F. L., Artandi, S. E. and Chang, H. Y.** (2011). Genomic maps of long noncoding RNA occupancy reveal principles of RNA-chromatin interactions. *Mol. Cell* **44**, 667-678.

**Fabian, D., Koppel, J. and Maddox-Hyttel, P.** (2005). Apoptotic processes during mammalian preimplantation development. *Theriogenology* **64**, 221-231.

**Farthing, C. R., Ficz, G., Ng, R. K., Chan, C.-F., Andrews, S., Dean, W., Hemberger, M. and Reik, W.** (2008). Global mapping of DNA methylation in mouse promoters reveals epigenetic reprogramming of pluripotency genes. *PLoS Genet.* **4**, e1000116.

**Fatica, A. and Bozzoni, I.** (2014). Long non-coding RNAs: new players in cell differentiation and development. *Nat. Rev. Genet.* **15**, 7-21.

**Gentleman, R. C., Carey, V. J., Bates, D. M., Bolstad, B., Dettling, M., Dudoit, S., Ellis, B., Gautier, L., Ge, Y., Gentry, J. et al.** (2004). Bioconductor: open software development for computational biology and bioinformatics. *Genome Biol.* **5**, R80.

**Gupta, R. A., Shah, N., Wang, K. C., Kim, J., Horlings, H. M., Wong, D. J., Tsai, M.-C., Hung, T., Argani, P., Rinn, J. L. et al.** (2010). Long non-coding RNA HOTAIR reprograms chromatin state to promote cancer metastasis. *Nature* **464**, 1071-1076.

**Hajkova, P., Jeffries, S. J., Lee, C., Miller, N., Jackson, S. P. and Surani, M. A.** (2010). Genome-wide reprogramming in the mouse germ line entails the base excision repair pathway. *Science* **329**, 78-82.

**Imamura, T., Neildez, T. M. A., Thenevin, C. and Paldi, A.** (2004a). Essential role for poly (ADP-ribosyl)ation in mouse preimplantation development. *BMC Mol. Biol.* **5**, 4.

**Imamura, T., Yamamoto, S., Ohgane, J., Hattori, N., Tanaka, S. and Shiota, K.** (2004b). Non-coding RNA directed DNA demethylation of Sphk1 CpG island. *Biochem. Biophys. Res. Commun.* **322**, 593-600.

**Imamura, T., Kerjean, A., Heams, T., Kupiec, J.-J., Thenevin, C. and Pàldi, A.** (2005). Dynamic CpG and non-CpG methylation of the Peg1/Mest gene in the mouse oocyte and preimplantation embryo. *J. Biol. Chem.* **280**, 20171-20175.

**Imamura, T., Uesaka, M. and Nakashima, K.** (2014). Epigenetic setting and reprogramming for neural cell fate determination and differentiation. *Philos. Trans. R. Soc. Lond. B Biol. Sci.* **369**, 20130511.

**Jadrich, J. L., O'Connor, M. B. and Coucouvanis, E.** (2006). The TGF beta activated kinase TAK1 regulates vascular development in vivo. *Development* **133**, 1529-1541.

**Kim, D., Pertea, G., Trapnell, C., Pimentel, H., Kelley, R. and Salzberg, S. L.** (2013). TopHat2: accurate alignment of transcriptomes in the presence of insertions, deletions and gene fusions. *Genome Biol.* **14**, R36.

**Kohli, R. M. and Zhang, Y.** (2013). TET enzymes, TDG and the dynamics of DNA demethylation. *Nature* **502**, 472-479.

**Latham, K. E., Garrels, J. I., Chang, C. and Solter, D.** (1991). Quantitative analysis of protein synthesis in mouse embryos. I. Extensive reprogramming at the one- and two-cell stages. *Development* **112**, 921-932.

**Liu, Y., Yan, X. and Zhou, T.** (2013). TBCK influences cell proliferation, cell size and mTOR signaling pathway. *PLoS ONE* **8**, e71349.

**Lois, C., Hong, E. J., Pease, S., Brown, E. J. and Baltimore, D.** (2002). Germline transmission and tissue-specific expression of transgenes delivered by lentiviral vectors. *Science* **295**, 868-872.

**Mayer, W., Niveleau, A., Walter, J., Fundele, R. and Haaf, T.** (2000). Embryogenesis: demethylation of the zygotic paternal genome. *Nature* **403**, 501-502.

**Meissner, A., Mikkelsen, T. S., Gu, H., Wernig, M., Hanna, J., Sivachenko, A., Zhang, X., Bernstein, B. E., Nusbaum, C., Jaffe, D. B. et al.** (2008). Genome-scale DNA methylation maps of pluripotent and differentiated cells. *Nature* **454**, 766-770.

**Mu, W., Munroe, R. J., Barker, A. K. and Schimenti, J. C.** (2010). PDCD2 is essential for inner cell mass development and embryonic stem cell maintenance. *Dev. Biol.* **347**, 279-288.

**Necsulea, A., Soumillon, M., Warnefors, M., Liechti, A., Daish, T., Zeller, U., Baker, J. C., Grützner, F. and Kaessmann, H.** (2014). The evolution of lncRNA repertoires and expression patterns in tetrapods. *Nature* **505**, 635-640.

**Oswald, J., Engemann, S., Lane, N., Mayer, W., Olek, A., Fundele, R., Dean, W., Reik, W. and Walter, J.** (2000). Active demethylation of the paternal genome in the mouse zygote. *Curr. Biol.* **10**, 475-478.

**Pages, H., Aboyoun, P., Gentleman, R. and DebRoy, S.** (2013). *Biostrings: String Objects Representing Biological Sequences, and Matching Algorithms*. R package version 2.32.0.

**Pall, G. S., Wallis, J., Axton, R., Brownstein, D. G., Gautier, P., Buerger, K., Mulford, C., Mullins, J. J. and Forrester, L. M.** (2004). A novel transmembrane MSP-containing protein that plays a role in right ventricle development. *Genomics* **84**, 1051-1059.

**Park, S.-J., Komata, M., Inoue, F., Yamada, K., Nakai, K., Ohsugi, M. and Shirahige, K.** (2013). Inferring the choreography of parental genomes during fertilization from ultralarge-scale whole-transcriptome analysis. *Genes Dev.* **27**, 2736-2748.

**Patel, R. K. and Jain, M.** (2012). NGS QC Toolkit: a toolkit for quality control of next generation sequencing data. *PLoS ONE* **7**, e30619.

**Rinn, J. L., Kertesz, M., Wang, J. K., Squazzo, S. L., Xu, X., Brugmann, S. A., Goodnough, L. H., Helms, J. A., Farnham, P. J., Segal, E. et al.** (2007). Functional demarcation of active and silent chromatin domains in human HOX loci by noncoding RNAs. *Cell* **129**, 1311-1323.

**Santos, F., Peters, A. H., Otte, A. P., Reik, W. and Dean, W.** (2005). Dynamic chromatin modifications characterise the first cell cycle in mouse embryos. *Dev. Biol.* **280**, 225-236.

**Sigova, A. A., Mullen, A. C., Molinie, B., Gupta, S., Orlando, D. A., Guenther, M. G., Almada, A. E., Lin, C., Sharp, P. A., Giallourakis, C. C. et al.** (2013). Divergent transcription of long noncoding RNA/mRNA gene pairs in embryonic stem cells. *Proc. Natl. Acad. Sci. USA* **110**, 2876-2881.

**Smallwood, S. A., Tomizawa, S.-i., Krueger, F., Ruf, N., Carli, N., Segonds-Pichon, A., Sato, S., Hata, K., Andrews, S. R. and Kelsey, G.** (2011). Dynamic CpG island methylation landscape in oocytes and preimplantation embryos. *Nat. Genet.* **43**, 811-814.

**Smith, Z. D., Chan, M. M., Mikkelsen, T. S., Gu, H., Gnirke, A., Regev, A. and Meissner, A.** (2012). A unique regulatory phase of DNA methylation in the early mammalian embryo. *Nature* **484**, 339-344.

**Strumpf, D., Mao, C.-A., Yamanaka, Y., Ralston, A., Chawengsaksophak, K., Beck, F. and Rossant, J.** (2005). Cdx2 is required for correct cell fate specification and differentiation of trophectoderm in the mouse blastocyst. *Development* **132**, 2093-2102.

**Teperek-Tkacz, M., Pasque, V., Gentsch, G. and Ferguson-Smith, A. C.** (2011). Epigenetic reprogramming: is deamination key to active DNA demethylation? *Reproduction* **142**, 621-632.

**Tomikawa, J., Shimokawa, H., Uesaka, M., Yamamoto, N., Mori, Y., Tsukamura, H., Maeda, K.-i. and Imamura, T.** (2011). Single-stranded noncoding RNAs mediate local epigenetic alterations at gene promoters in rat cell lines. *J. Biol. Chem.* **286**, 34788-34799.

**Trapnell, C., Roberts, A., Goff, L., Pertea, G., Kim, D., Kelley, D. R., Pimentel, H., Salzberg, S. L., Rinn, J. L. and Pachter, L.** (2012). Differential gene and transcript expression analysis of RNA-seq experiments with TopHat and Cufflinks. *Nat. Protoc.* **7**, 562-578.

**Tsai, M.-C., Manor, O., Wan, Y., Mosammaparast, N., Wang, J. K., Lan, F., Shi, Y., Segal, E. and Chang, H. Y.** (2010). Long noncoding RNA as modular scaffold of histone modification complexes. *Science* **329**, 689-693.

**Uesaka, M., Nishimura, O., Go, Y., Nakashima, K., Agata, K. and Imamura, T.** (2014). Bidirectional promoters are the major source of gene activation-associated non-coding RNAs in mammals. *BMC Genomics* **15**, 35.

**Wang, L., Zhang, J., Duan, J., Gao, X., Zhu, W., Lu, X., Yang, L., Zhang, J., Li, G., Ci, W. et al.** (2014). Programming and inheritance of parental DNA methylomes in mammals. *Cell* **157**, 979-991.

**Yeh, W.-C., de la Pompa, J. L., McCurrach, M. E., Shu, H.-B., Elia, A. J., Shahinian, A., Ng, M., Wakeham, A., Khoo, W., Mitchell, K. et al.** (1998). FADD: essential for embryo development and signaling from some, but not all, inducers of apoptosis. *Science* **279**, 1954-1958.

**Ying, Q.-L., Wray, J., Nichols, J., Batlle-Morera, L., Doble, B., Woodgett, J., Cohen, P. and Smith, A.** (2008). The ground state of embryonic stem cell self-renewal. *Nature* **453**, 519-523.

**Younglai, E. V., Holt, D., Brown, P., Jurisicova, A. and Casper, R. F.** (2001). Sperm swim-up techniques and DNA fragmentation. *Hum. Reprod.* **16**, 1950-1953.

**Zhou, Z., Hong, E. J., Cohen, S., Zhao, W.-N., Ho, H.-Y. H., Schmidt, L., Chen, W. G., Lin, Y., Savner, E., Griffith, E. C. et al.** (2006). Brain-specific phosphorylation of MeCP2 regulates activity-dependent Bdnf transcription, dendritic growth, and spine maturation. *Neuron* **52**, 255-269.

frontiers in Cellular Neuroscience

ORIGINAL RESEARCH
published: 29 January 2016
doi: 10.3389/fncel.2016.00009

# Paired Burst Stimulation Causes $GABA_A$ Receptor-Dependent Spike Firing Facilitation in CA1 of Rat Hippocampal Slices

*Takashi Tominaga* and Yoko Tominaga*

*Laboratory for Neural Circuit Systems, Institute of Neuroscience, Tokushima Bunri University, Sanuki, Japan*

The theta oscillation (4–8 Hz) is a pivotal form of oscillatory activity in the hippocampus that is intermittently concurrent with gamma (25–100 Hz) burst events. In *in vitro* preparation, a stimulation protocol that mimics the theta oscillation, theta burst stimulation (TBS), is used to induce long-term potentiation. Thus, TBS is thought to have a distinct role in the neural network of the hippocampal slice preparation. However, the specific mechanisms that make TBS induce such neural circuit modifications are still unknown. Using electrophysiology and voltage-sensitive dye imaging (VSDI), we have found that TBS induces augmentation of spike firing. The augmentation was apparent in the first couple of brief burst stimulation (100 Hz four pulses) on a TBS-train in a presence of NMDA receptor blocker (APV 50 μM). In this study, we focused on the characterizes of the NMDA independent augmentation caused by a pair of the brief burst stimulation (the first pair of the TBS; paired burst stimulation-PBS). We found that PBS enhanced membrane potential responses on VSDI signal and intracellular recordings while it was absent in the current recording under whole-cell clamp condition. The enhancement of the response accompanied the augmentation of excitatory postsynaptic potential (EPSP) to spike firing (E-S) coupling. The paired burst facilitation (PBF) reached a plateau when the number of the first burst stimulation (priming burst) exceeds three. The interval between the bursts of 150 ms resulted in the maximum PBF. Gabazine (a $GABA_A$ receptor antagonist) abolished PBF. The threshold for spike generation of the postsynaptic cells measured with a current injection to cells was not lowered by the priming burst of PBS. These results indicate that PBS activates the GABAergic system to cause short-term E-S augmentation without raising postsynaptic excitability. We propose that a GABAergic system of area CA1 of the hippocampus produce the short-term E-S plasticity that could cause exaggerated spike-firing upon a theta-gamma activity distinctively, thus making the neural circuit of the CA1 act as a specific amplifier of the oscillation signal.

**Keywords: hippocampus, theta, voltage-sensitive dye, $GABA_A$ receptor**

OPEN ACCESS

***Edited by:***
*Andrea Nistri,*
*SISSA: International School for Advanced Studies, Italy*

***Reviewed by:***
*Afia B. Ali,*
*UCL School of Pharmacy, UK*
*Renato Corradetti,*
*University of Florence, Italy*

****Correspondence:***
*Takashi Tominaga*
*tominagat@kph.bunri-u.ac.jp*

***Received:*** *04 November 2015*
***Accepted:*** *11 January 2016*
***Published:*** *29 January 2016*

***Citation:***
*Tominaga T and Tominaga Y (2016) Paired Burst Stimulation Causes $GABA_A$ Receptor-Dependent Spike Firing Facilitation in CA1 of Rat Hippocampal Slices. Front. Cell. Neurosci. 10:9. doi: 10.3389/fncel.2016.00009*

## INTRODUCTION

Oscillatory neuronal activity plays pivotal roles in brain function (Buzsáki, 2006; Paulsen and Sejnowski, 2006; Sejnowski and Paulsen, 2006; Bartos et al., 2007; Fries et al., 2007). The concomitant occurrence of high- and low- frequency oscillations in many regions of the brain might work in concert to provide information to the neural network (Buzsáki and da Silva, 2012). Oscillations are a means for constructing spike firing patterns that encode information underlying distinct neuronal functions (Singer and Gray, 1995; Tiesinga et al., 2008). In the hippocampus, theta oscillations (4–8 Hz), such observed in animal exploration and learning (O'Keefe and Dostrovsky, 1971), occur together with gamma oscillations (25–100 Hz) to enable gamma-theta coding that plays a critical role (Buzsáki, 2002, 2005). Indeed, theta oscillations accompany spike generation in pyramidal cells (Ranck, 1973); the timing of which corresponds to basal oscillations critical for information encoding (O'Keefe and Recce, 1993).

An *in vitro* model of patterned stimulation that mimics theta oscillations (theta burst stimulation (TBS); TBS (a train of brief 100 Hz burst stimulations repeated in 5–7 Hz)) was found to induce long-term synaptic potentiation (LTP) at excitatory synapses (Larson and Lynch, 1986; Larson et al., 1986; Huerta and Lisman, 1995; Larson and Munkácsy, 2015). LTP induced by TBS is different from that caused by a "tetanic" high-frequency stimulus (HFS) in that these two forms of LTP exhibit different sensitivities to regulatory factors such as BDNF (Korte et al., 1995, 1996; Kang et al., 1997; Chen et al., 1999; Edelmann et al., 2015) and Ab42 (Smith et al., 2009). The mechanism of the difference is still not fully understood (Larson and Munkácsy, 2015). We have found differences in neuronal responses to these patterned stimuli during the induction stimulation of LTP. A 100 Hz HFS inhibited spike generation during the period of stimulation, on the contrary, TBS augmented spikes during the period of TBS train from the first pair of the brief burst stimulation (Tominaga et al., 2002).

These short-term modifications of synaptic responses occurred in the presence of NMDA-receptor inhibitor (APV 50 μM) and were reproducible within a short interval with any long-term modification. We showed that the short-term plasticity caused by HFS was dependent on GABA$_A$ receptor (Tominaga and Tominaga, 2010). The augmentation of spike firing during TBS can be caused by the modification excitatory postsynaptic potential (EPSP) to spike generation (excitation-spike, E-S) coupling similar to that caused in parallel to the LTP induction (E-S potentiation; Andersen et al., 1980; Abraham et al., 1987; Chavez-Noriega et al., 1989, 1990; reviewed by Daoudal and Debanne, 2003). While the latter is a long-term plasticity, comparison of the controlling mechanisms of spike generation should be important. The ability of TBS to control action potential firing likely plays a critical role in controlling plasticity, as firing properties have great importance in plasticity by timing action potentials and controlling synaptic strength (Markram et al., 1997; Bi and Poo, 1998; Song et al., 2000).

On the other hand, since the short-term augmentation by TBS was apparent at the first pair of the burst stimulation, similarity to the well-known short-term plasticity of the paired pulse facilitation (PPF; Creager et al., 1980; McNaughton, 1980, 1982) should also be pursuit. It is also interesting to seek the short-term plasticity mechanism that can explain the longer range of time window than 30–60 ms of PPF applicable to theta range of events.

We recently found that high-frequency stimulation (100 Hz) induced GABA$_A$-receptor-dependent long-lasting depolarization, which in turn inhibits excitatory neural signal propagation around the stimulating electrode (Tominaga and Tominaga, 2010) during HFS. Because TBS consists of the same 100 Hz burst while it is very brief (only 4–5 pulses), it is possible that same GABAergic modification caused TBS-induced short-term plasticity through the short-term plastic change of the GABAergic system (reviewed by Kaila et al., 2014a,b).

We, therefore, aimed to explore the neuronal mechanisms by which TBS regulates spike firing in a simple single input *in vitro* model of gamma-theta interactions. We further tested for the possible involvement of GABA$_A$-receptor-mediated action potential firing control, which would represent a network driven mechanism of TBS regulation of neuronal activity.

## MATERIALS AND METHODS

### Slice Preparation and Staining with VSD

All animal experiments were performed according to protocols approved by the Animal Care and Use Committee of Tokushima Bunri University. Hippocampal slices were prepared from 4-5-week-old male Wistar rats that were decapitated under deep isoflurane anesthesia after perfusion with ice-cold artificial cerebrospinal fluid (aCSF; 124 mM NaCl, 2.5 mM KCl, 2 mM $CaCl_2$, 2 mM $MgSO_4$, 1.25 mM $NaH_2PO_4$, 26 mM $NaHCO_3$, and 10 mM glucose; pH 7.4) bubbled with 95%/5% $O_2/CO_2$ gas. The brains were quickly removed and cooled in aCSF. After cooling for 5 min, the hippocampus and surrounding cortex were dissected and sliced into 400 μm transverse sections using a vibratome (Leica VT-1000 or VT-1200S). Following incubation in gassed aCSF for 3–5 min, each slice was transferred onto a fine-mesh membrane filter (Omni Pore membrane filter, JHWP01300; Millipore Corp., MA, USA) held in place by a thin Plexiglas ring (inner diameter, 11 mm; outer diameter, 15 mm; thickness 1–2 mm). These slices were transferred to a moist chamber continuously supplied with a humidified $O_2/CO_2$ gas mixture. The temperature was held at 32°C for 1 h, and then maintained at room temperature thereafter.

After 1 h of incubation, each slice was stained for 25 min with 100 μl of voltage sensitive dye (VSD) solution containing 0.2 mM Di-4-ANEPPS (Molecular Probes) in 2.5% ethanol, 0.13% Cremophor EL (Sigma), 1.17% distilled water, 48.1% fetal bovine serum (Sigma), and 48.1% ACSF. After washing to remove VSD, sections were incubated at room temperature for least 1 h before they were imaged by optical recording.

## Optical Recording

The Plexiglas ring supporting each slice was placed in an immersion-type recording chamber. Slices were continuously perfused with pre-warmed (31°C) and oxygenated aCSF (bubbled with a 95%/5% $O_2/CO_2$ gas mixture) at a rate of 1 ml/min. Custom laboratory-designed epifluorescence optics consisting of two principal lenses were used to view the slices during experiments. The optics consisted of a custom-made objective lens (Olympus MYCAM 5×/0.6 WI; the final magnification of the system was 5×) as the objective lens, and a ($f$ = 55 mm × 1.0) Leica Microsystems MZ-APO lens as the projection lens. Excitation light was provided by a halogen lamp source (150 W; MHW-G150LR; Moritex Corp.) and was projected through an excitation filter ($\lambda$ = 530 ± 10 nm) and reflected onto the hippocampal slice by a dichroic mirror ($\lambda$ = 575 nm). Emission fluorescence from the slice was passed through an emission filter ($\lambda$ > 590 nm) and projected onto a CCD camera (MiCAM01 and MiCAM Ultima; BrainVision, Inc., Tokyo, Japan). The high-speed imaging system provided a spatial resolution of approximately 22 × 22 μm at the objective (96 pixels × 64 pixels resolution; MiCAM01) and 18.2 × 18.2 μm (100 pixels × 100 pixels resolution; MiCAM Ultima).

The intensity of emitted slice fluorescence prior to stimulation (a pre-stimulation period usually lasted 40 frames) was averaged and used as a reference intensity ($F_0$). The fractional change in fluorescence [$\Delta F(t) = F(t) - F_0$] was normalized by $F_0$ ($\Delta F/F_0$), and this value was used as the optical signal. Optical signals referred to in the following sections represent signals filtered in spatial and temporal dimensions with a Gaussian kernel of 5 × 5 × 3 (horizontal × vertical × temporal).

We analyzed optical signals offline using a procedure developed for IgorPro (WaveMetrics Inc., OR, USA). At a wavelength of 610 nm, VSD fluorescence decreases in response to the depolarization of the membrane. To fit the polarity of the response to conventional membrane potential changes, we expressed the optical signal in a polarity that matched the membrane potential change. For example, decreased fluorescence, which corresponds to depolarization, was represented as a positive deflection. For additional details on the methods, see Tominaga et al. (2000, 2002).

## Electrophysiological Recording and Stimulation

Patch-clamp recordings in whole-cell mode were obtained using a patch-clamp amplifier with a capacitive headstage (Axoclamp 700B; Axon Instruments, Foster City, CA, USA). Pipettes of borosilicate glass (Sutter Instruments, Novato, CA, USA) were pulled using a P-97 Flaming-Brown pipette puller (Sutter Instruments, Novato, CA, USA). The Cs-based pipette internal solution used for whole-cell voltage clamp experiments consisted of (in mM): 130 Cs-$MeSO_3$, 10 HEPES, 4 $MgCl_2$, 4 NaATP, 0.4 NaGTP, 10 Na-phosphocreatine, 10 EGTA; pH was adjusted to 7.2; 5 mM QX-314 was also added (2–4 MΩ).

Whole-cell recordings were low-pass-filtered at 3 kHz and digitized at 10 kHz (ITC-18; InstruTech Inc., NY, USA). Data were fed into an Apple computer for on-line and off-line analysis using laboratory-developed software on IgorPro (WaveMetrics Inc., OR, USA). Electrical stimuli were constant current pulses (A395, WPI) applied through a glass microcapillary pipette (5 μm inner diameter; filled with aCSF). Neurons were visualized by oblique illumination with the aid of contrast enhancement provided by a CMOS camera (SKDCE-2EX; Sigma Koki Co., Tokyo, Japan) attached to an upright microscope (BX-51WI; Olympus Tokyo, Japan). In voltage-clamp mode, a test membrane potential step (−10 mV) was always applied prior to electrical stimulation, and traces with series resistance (Rs) lower than 25 MΩ were accepted. Membrane current at the holding potential of −70 mV were presented.

For intracellular recording, we used a fine-tipped glass microelectrode filled with 4 M potassium acetate (approximately 100 MΩ). An Axoclamp-2B amplifier (Axon Instruments) was used in continuous bridge mode. Cells with resting potentials of −65 to −80 mV were accepted for study.

Stimulation electrode was placed in the middle of the stratum radiatum (about 200 μm from the startum pyramidale) at the border between the CA1 and CA3. Whole cell recordings and intracellular recordings were applied to the cells in the middle of CA1 (about 500 μm from the stimulating electrode).

The electrophysiological recording system was controlled by a procedure developed in Igor Pro (WaveMetrics Inc., OR, USA). Artifacts caused by electrical stimulation were digitally removed from the traces shown in the Results. To monitor synaptic transmission in CA1 we applied a 0.05–0.1 Hz stimulus at an intensity that produced an approximately 30% maximal field excitatory postsynaptic potential (fEPSP).The fEPSPs were always monitored with a field potential electrodes placed at the most distal end of the area CA1 in all the experiments. A laboratory-made differential amplifier and a general-purpose amplifier (model 440; Brownlee Precision, San Jose, CA, USA) were used for field potential recordings. A glass microcapillary pipette (5 μm inner diameter; filled with aCSF) was used as a recording electrode for field potential recordings. The electrophysiological recording and the optical recording did not interfere with each other.

## Drugs and Solutions

All experiments were conducted in the presence of 50 μM DL-2-amino-5-phosphonovaleric acid (APV, Tocris), unless otherwise stated. We took advantage of the absence of synaptic plasticity effects in the presence of APV to apply multiple episodes of tetanic stimulation in a single slice and to improve the signal-to-noise (S/N) ratio of optical signals by averaging. SR95531 (gabazine) was dissolved in water to make a 10 mM stock solution. Other common reagents were obtained through local resellers in Japan.

## Data Analysis

Optical and electrophysiological signals were analyzed using custom macro programs on Igor Pro (WaveMetrics Inc., OR, USA). All data are expressed as the mean ± SEM; and $n$ represents the number of slices. Statistical significance was

tested with Tukey's mutiple comparisons after one-way analysis of variance (ANOVA) using Igor Pro (WaveMetrics Inc., OR, USA).

## RESULTS

### Paired Burst Transiently Increased Postsynaptic Membrane Potential Responses in CA1 Pyramidal Cells upon Schaffer Collateral Stimulation

We first sought to understand the effect of neural activity similar to theta-bursts on facilitation in the hippocampus. A set of four pulses of burst stimulation (100 Hz) to the Schaffer collateral pathway with subthreshold stimulus intensity did not elicit spikes under sharp electrode intracellular recording (**Figure 1B** stimulation I). However the same set of four pulses of burst stimulation at same stimulus intensity after 170 ms (stimulation II) elicited spike firing (**Figure 1B** stimulation II). Hereafter we used this paired burst stimulation (PBS) pattern [a 100 Hz burst stimulation consists of four stimuli with10 ms interval (a priming burst; I) proceeds 170 ms of interburst interval to the same 100 Hz burst stimulation (a test burst; II)] illustrated in the **Figures 1B,C** as a PBS unless otherwise stated. The PBS of 170 ms of interburst interval is identical to the first pair of the TBS. This result is consistent with a finding that a train of burst stimuli that mimics theta-burst TBS showed progressive facilitation of action potential generation (Tominaga et al., 2002). Please note that the response to the PBS and monitoring fEPSPs to single stimulation were consistent at least when the PBS applied every 20 s, so that the facilitation did not last more than 20 s. We next examined the response to the same PBS paradigm throughout the slice by analyzing optical signals using a VSD imaging method. We observed that augmentation of the postsynaptic responses occurred in both the stratum pyramidale (SP) (**Figure 1C** top trace) and stratum radiatum (SR) (**Figure 1C** bottom trace) across most of CA1 (**Figure 1D**). We evaluated the amplitude of the response to each stimulus (1–4) of the priming burst stimulus (I in the **Figures 1B–E**) and the following test burst stimulus (II) by measuring peak amplitude of the response in the middle of the stratum radiatum. As shown in **Figure 1E**, the responses to the test burst (filled bars) were significantly larger than those to the priming burst (open bar) in the 3rd and 4th stimulus. Since a pair of 100 Hz burst stimulation caused transient facilitation of the response to the subsequent burst stimulation, we refer this short-term plastic change in postsynaptic response as a paired burst facilitation (PBF).

We next asked whether the PBF is caused by the modification of the synaptic transduction by whole cell clamp experiments. Excitatory postsynaptic current (EPSC) were measured with whole cell clamp condition with the internal solution adjusted to minimize inhibitory current at the holding potential of −70 mV ($E_{Cl}$ = −70 mV). There were no significant difference between the postsynaptic responses in the priming burst (I) and test burst (II) under voltage clamp conditions (**Figures 1F,G**). Therefore, the PBF was specific to membrane potential responses and not due to increased synaptic receptor currents.

### PBF Accompanied Transient Augmentation of Excitation-Spike (E-S) Coupling

Given that TBS has been shown to increase the chance of spike firing (Tominaga et al., 2002), we examined the relationship between synaptic potential and spike-firing during PBF. Facilitation in the magnitude of the optical responses in CA1 was observed in response to a range of stimulus intensities (**Figures 2A,B**).

Plotting the relationships between the response in the SR and SP in the control condition (without priming burst; black symbols) and in the test condition (with priming burst; blue symbols) revealed a linear relationship in both regions (**Figure 2C**). Moreover, the slopes were higher with a priming burst than without priming.

The optical signal in the SR is dependent on EPSP, while in the SP is dependent on the spike occurrence (Tominaga et al., 2009). Thus, the larger slope elicited with the PBS condition implies there was an enhanced excitation-spike (E-S) firing relationship (i.e., augmentation of E-S coupling). Therefore, we here-to-fore use the ratio of the response of the SP and that of the SR (PR-ratio) as a measure of the strength of the E-S relationship (Tominaga et al., 2009). The PR-ratio in the test condition (+ burst) was significantly larger than the control (−burst; **Figure 2D**). That is, PBF accompanied transient short-term modification of E-S coupling. By contrast, the same relationships measured using the well-established short-term plasticity caused by the PPF protocol (Creager et al., 1980; McNaughton, 1980, 1982) did not exhibit changes in the PR-ratio (**Figure 2E**). Thus, the PBF might require different mechanisms than well-established forms of PPF caused by the presynaptic mechanisms (Manabe et al., 1993; Manabe and Nicoll, 1994).

### Effect of the Number of the Priming Burst and Interburst Interval of PBS

We next assessed if PBF caused by "burst" stimuli affected facilitation and found that optical signals increased to their maximum values with either three or four priming burst stimulations (one to six stimuli were tested; **Figure 3A**). The maximum amplitude was observed in response to the third stimulation in SR and SP. Facilitation was highest when there were four stimulations. The PR-ratio increased as the number of the priming burst stimulations increased, until reaching the peak value at four stimulations (**Figure 3C**).

We next tested the optical signals elicited by PBS at different interburst intervals (**Figure 3D**). The amplitude of the response and E-S potentiation reflected in the PR-ratio were greatest when the interval was approximately150 ms (**Figures 3E,F**).

### PBF is Dependent on GABA$_A$-Receptor Activation

A 100 Hz stimulation is known to cause reversal of GABA$_A$-receptor currents from hyperpolarizing to depolarizing

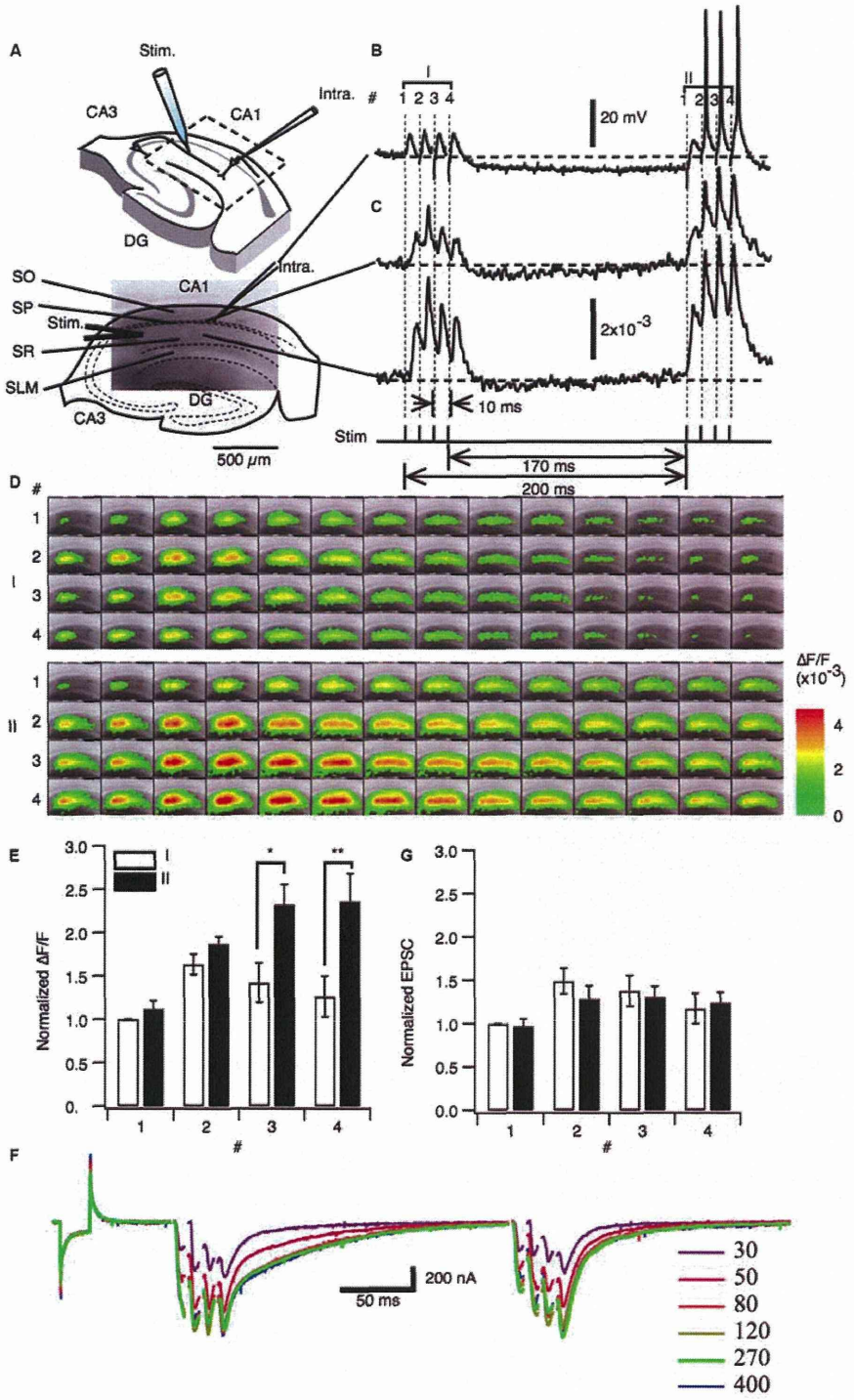


**FIGURE 1 | Paired priming burst stimulation increased excitatory postsynaptic transmission in later burst stimulations. (A)** Upper image: Schematic illustration of a hippocampal slice with a stimulation electrode (Stim). A field of view of the optical recording is shown in the image embedded in the square inset. The image in the lower panels shows a fluorescent image (ca. 2 mm × 1.3 mm) of the area of CA1 imaged by optical recording. Abbreviations: SO, stratum oriens-alveus; SP, stratum pyramidale; SR, stratum radiatum; SLM, stratum lacunosum-moleculare. **(B)** Representative intracellular membrane potential trace recorded with a sharp microelectrode. **(C)** Representative optical signal of a pixel acquired from the stratum pyramidale (upper panel) and a pixel acquired from the

(*Continued*)

**FIGURE 1 | Continued**
*middle of the stratum radiatum (lower panel).* Protocol of the paired burst stimulation are shown in the bottom of **(C)**. The stimulation consisted of the priming burst stimulation (I: 100 Hz 4 pulses) and the test burst stimulation (II: 100 Hz 4 pulses) with 170 ms interval. **(D)** Sets of consecutive images of optical signals sampled every 0.7 ms for the priming burst stimulation (I) and the test burst stimulation burst (II) of stimulation numbers 1–4 (top to bottom). **(E)** Amplitude of the optical response upon test simulation (I; open bars) and the following stimulation burst (II; filled bars; mean ± SEM; $*p < 0.05$, $**p < 0.01$; $n = 6$). **(F)** Membrane current response under whole-cell clamp conditions (holding potential = −70 mV) at different stimulus intensities. **(G)** Amplitude of the EPSCs recorded for the burst stimuli (I) and (II). (mean ± SEM; $n = 5$).

membrane potential responses (Buzsáki et al., 2007; Kaila et al., 2014a) and cause several short-term plasticity in area CA1 (Tominaga and Tominaga, 2010). Thus, PBS might be achieved through a GABA$_A$-receptor-mediated mechanism. We tested this by applying GABA$_A$ a receptor antagonist to the hippocampal slice media and assessing neural activity (SR95531 or gabazine, 10 μM; **Figure 4**). Application of gabazine could cause saturation of the response so that we tested responses

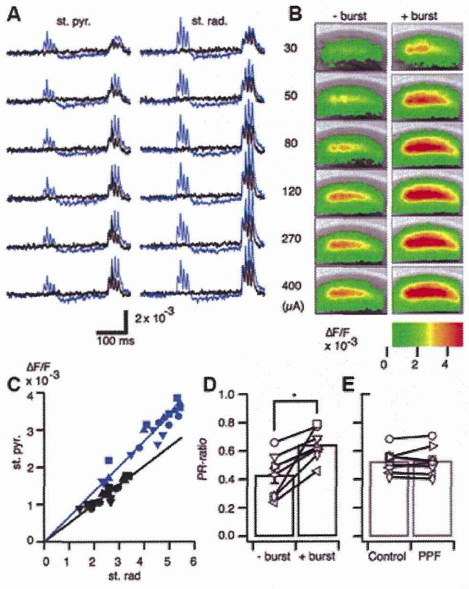


**FIGURE 2 | Excitation-spike generation potentiation caused by paired burst facilitation. (A)** Representative traces of optical signals acquired from the stratum pyramidale (st. pyr.) and stratum radiatum (st. rad.) at stimulus intensities of 30, 50, 80, 120, 270, and 400 μA with (blue) and without (black) a priming burst stimulation. **(B)** Pseudo-colored image of the projection of the maximum amplitude of the response to the burst stimulation without a priming burst (−burst) and with a priming burst (+burst) at each of the stimulus intensities. **(C)** Representative relationship of the optical signal amplitude in the stratum pyramidale and stratum radiatum without a priming burst (black) and with a priming burst (blue). **(D)** Ratio of the response in the stratum pyramidale and stratum radiatum (PR-ratio; $*p < 0.01$; $n = 8$). **(E)** The same analysis as in **(D)** conducted for the paired-pulse facilitation protocol (inter-stimulus interval = 40 ms); no significant differences were found between the single stimulus and paired stimulus conditions.

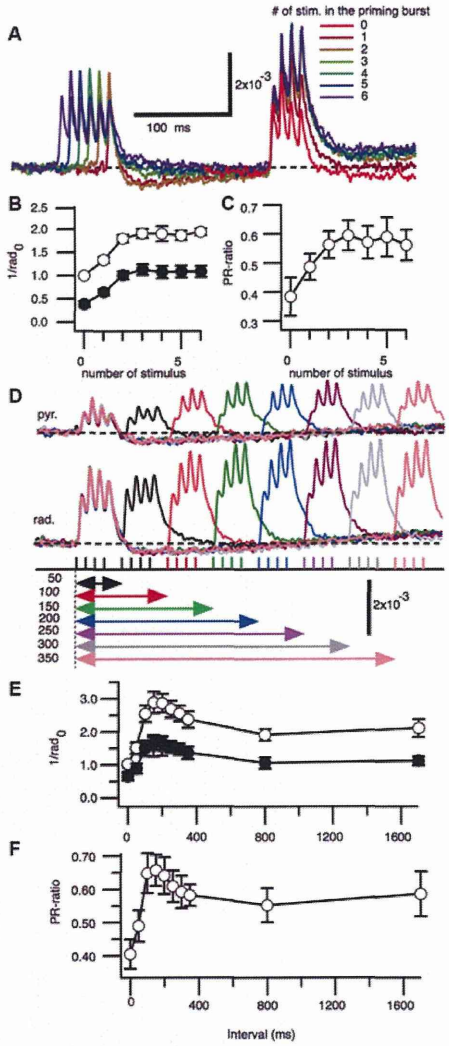


**FIGURE 3 | Effect of increasing numbers of burst stimulations and burst repetition intervals on the facilitation of excitatory synaptic transmission. (A)** Superimposed representative traces of the optical signals acquired from the stratum radiatum after zero to six burst stimulations. The amplitude of the third peak of the response was measured. **(B)** Pooled data for the amplitude of the test responses normalized by the control response (no priming burst stimulation) at the stratum radiatum ($1/rad_0$) in the stratum pyramidale and stratum radiatum, as a function of the number of priming bursts. **(C)** Ratio of the stratum pyramidale and stratum radiatum amplitudes as a function of the priming burst ($n = 6$). **(D)** Representative set of optical signals acquired from the stratum pyramidale (st. pyr.) and stratum radiatum (st. rad.) at different burst intervals (50–350 ms). **(E)** Change in the normalized maximum amplitude [normalized by the control response (no priming burst stimulation) at the stratum radiatum ($1/rad_0$) of the test burst stimulation as a function of burst intervals. **(F)** Ratio of the response between the stratum pyramidale and stratum radiatum (PR-ratio) as a function of burst intervals ($n = 5$; Bars indicate the SEM).

in normal ACSF and inhibitor-treated ACSF at different stimulus intensities with or without priming burst stimulation (+burst vs. -burst; **Figures 4A,B**; stimulation intensity of the priming burst was 100 μA). That is clear when comparing